CCFE
CULHAM CENTRE FOR FUSION ENERGY

UK Atomic Energy Authority

UKAEA-CCFE-PR(25)342

D. Moseev, R. Ochoukov, M. Dreval, I. Kuzmych, P. Aleynikov, K. Aleynikova, S. Bozhenkov, R. Dendy, D. Hartmann, J.-P. Kallmeyer, Ye. O. Kazakov, L. Krier, H.P. Laqua, S. Marsen, K. McClements, J. Ongena, J.W. Oosterbeek, S. Ponomarenko, B. Reman, J. Riemann, M. Salewski, O. Samant, D. Straus, T. S. Schmidt, F. Schröder, B. Schweer, T. Stange, R.C. Wolf, J. Zimmermann, W7-X Team

Ion cyclotron emission from ECRH-heated plasmas in Wendelstein 7-X

Ion cyclotron emission from ECRH-heated plasmas in Wendelstein 7-X

D. Moseev, R. Ochoukov, M. Dreval, I. Kuzmych, P. Aleynikov, K. Aleynikova, S. Bozhenkov, R. Dendy, D. Hartmann, J.-P. Kallmeyer, Ye. O. Kazakov, L. Krier, H.P. Laqua, S. Marsen, K. McClements, J. Ongena, J.W. Oosterbeek, S. Ponomarenko, B. Reman, J. Riemann, M. Salewski, O. Samant, D. Straus, 1, 8 B.S. Schmidt, T. Schröder, B. Schweer, T. Stange, R.C. Wolf, J. Zimmermann, W7-X Team

This is a preprint of a paper submitted for publication in Physics of Plasmas

Ion cyclotron emission from ECRH-heated plasmas in Wendelstein 7-X

D. Moseev,[1] R. Ochoukov,[1] M. Dreval,[2] I. Kuzmych,[1,3] P. Aleynikov,[1] K. Aleynikova,[1] S. Bozhenkov,[1] R. Dendy,[4] D. Hartmann,[1] J.-P. Kallmeyer,[1] Ye. O. Kazakov,[5] L. Krier,[1] H.P. Laqua,[1] S. Marsen,[1] K. McClements,[6] J. Ongena,[5] J.W. Oosterbeek,[1] S. Ponomarenko,[1] B. Reman,[5] J. Riemann,[1] M. Salewski,[7] O. Samant,[6] D. Straus,[1,8] B.S. Schmidt,[9] T. Schröder,[1] B. Schweer,[5] T. Stange,[1] R.C. Wolf,[1] J. Zimmermann,[1] and W7-X Team

[1)] *Max-Planck Institute for Plasma Physics, Greifswald and Garching, Germany*

[2)] *Institute of Plasma Physics, National Science Center, Kharkov Institute of Physics and Technology, 61108 Kharkov, Ukraine*

[3)] *V.N. Karazin Kharkiv National University, Svobody sq. 4, 61022 Kharkiv, Ukraine*

[4)] *Centre for Fusion, Space and Astrophysics, University of Warwick, Coventry CV4 7AL, UK*

[5)] *Laboratory for Plasma Physics, LPP-ERM/KMS, TEC Partner, 1000 Brussels, Belgium*

[6)] *United Kingdom Atomic Energy Authority, Culham Campus, Abingdon, Oxfordshire, United Kingdom of Great Britain and Northern Ireland*

[7)] *Department of Physics, Technical University of Denmark, Kgs. Lyngby 2800, Denmark*

[8)] *University of Toronto, Canada*

[9)] *University of California Irvine, Department of Physics and Astronomy, 4129 Frederick Reines Hall, Irvine, CA, US 92697*

(*Electronic mail: dmitry.moseev@ipp.mpg.de)

(Dated: 10 September 2025)

We report the observation and analysis of ion cyclotron emission (ICE) in the Wendelstein 7-X (W7-X) stellarator during discharges without a significant fast-ion population. In these experiments, ICE is observed using the strap of the ICRF antenna, while remaining undetectable on the B-dot probes during ECRH-only phases. At low electron densities, the ICE signal on the ICRF strap exhibits an exponential increase in time, ultimately leading to diagnostic saturation, coinciding with the absence of low-frequency MHD activity and a rise in energy transport. Although a causal relationship cannot be firmly established, the correlation is striking. The ICE spectrum also displays multiple local maxima spaced by ≈700 kHz; simulations based on Kolesnichenko's model suggest that the origin of the ICE is outside of the last closed flux surface (LCFS). While the model can be used for studying the observations in hydrogen, it fails to describe ICE in helium discharges, where the signal peaks at 41 MHz instead of the expected 17MHz.

I. INTRODUCTION

Most observations and interpretation of ion cyclotron emission (ICE) from magnetically confined tokamak[1–30], stellarator[31–36] and cylindrical[37] plasmas relate to strongly suprathermal signals driven by minority energetic ion populations whose velocity-space distributions deviate strongly from a Maxwellian. Examples of such populations include fusion-born ions[1,3,6,7,11,22,26,27] within Ohmic and additionally heated plasmas, together with neutral beam injected (NBI) ions[9,13,15,17,18,24,26,38] and ion cyclotron resonance heated (ICRH) minorities[38,39]. Suprathermal ICE has provided a highly sensitive detector of the presence of fusion-born ions at very low concentrations $< 10^{-7}$: examples include Ohmic plasmas in JET, see for example Fig.5 of Cottrell[4], and unanticipated sub-populations of 3MeV protons born in deuterium plasmas in the KSTAR tokamak[11,13] and LHD heliotron-stellarator[32,33] . In the present paper, our focus is observations of suprathermal ICE from hydrogen and helium plasmas in the Wendelstein 7-X (W7-X) stellarator, in which no energetic ions are present. Specifically, in the plasmas studied here, there are: no externally applied or internally induced (for example, by reconnection) electric fields that might accelerate ions; no fusion-born ions, since hydrogen is highly inert in this respect; and no energetic ions from NBI or ICRH, neither of which is applied. It follows that only the thermal population of ions can generate the observed signal, whose spectral structure incorporates ion cyclotron frequency features. We therefore refer to this phenomenon hereafter as thermal population ion cyclotron emission (TPICE). Seemingly similar signals were observed in MAST Upagrade[40], where ICE emission was detected in the absence of auxiliary heating and was only visible by the Doppler back-scattering diagnostic and not by fast Mirnov coils. However, there the observations were attributed to the generation of small fractions of fast ions in the reconnection events.

The TPICE of the electromagnetic nature were observed in JT-60U[41] and Tuman-3M[42].

This paper is organized as follows. Section II provides an overview of Wendelstein 7-X and the experimental setup used for ICE measurements. The possible nature of TPICE is discussed in Section III. Section IV presents the experimental observations of ICE under various plasma conditions. A possible interpretation of these observations is offered in Section V. Finally, Section VI summarizes the main findings of the paper.

II. SETUP

Wendelstein 7-X is an optimized quasi-isodynamic stellarator with five-fold toroidal symmetry. It has an aspect ratio of $R/r_a \approx 10$ and a major radius of $R \approx 5.5$ m. The device is currently equipped with up to 9 MW of steady-state-capable elec-

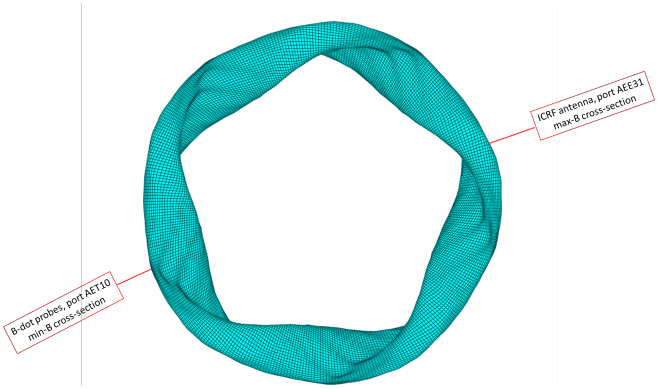

FIG. 1. A sketch showing the first wall of Wendelstein 7-X and the relative locations of ICE detectors in the stellarator.

tron cyclotron resonance heating (ECRH), 7 MW of neutral beam injection (NBI) power, and a 2 MW ion cyclotron resonance frequency (ICRF) heating system, which is presently being commissioned. Key results from Wendelstein 7-X can be found in the following publications[43–48].

A detailed description of the ICE diagnostic is provided in reference[49]. Briefly, the system includes four B-dot probes (three operational, one damaged) installed behind the heat shield of the CTS diagnostic, such that they do not face the plasma directly. The probes are connected via 25 dB amplifiers to an analog-to-digital converter (ADC) with a sampling rate of 1 GS/s and 14-bit resolution, using 25 m long triaxial Ultraflex-10 cables. In addition, one strap of the ICRF antenna is connected to the same ADC through a 10 dB attenuator located at the measurement disconnect terminal. After attenuation, the signal is transmitted via 72 m of triaxial Ultraflex-10 cable, following a similar path to the B-dot probe signals. The ICRF antenna is not protected by a Faraday shield and, although grounded, is sensitive to high-frequency electrostatic pickup as well as magnetic field fluctuations.

The relative locations of the ICE detectors are shown in figure 1. The detectors are installed on opposite sides of the torus and in regions with different magnetic field strengths: the B-dot probes are located in the AET10 port, near a cross-section with minimum average magnetic field, while the ICRF antenna in the AEE31 port is positioned near a maximum-field cross-section.

The data is sampled in 20 μ s intervals every millisecond. For spectral analysis, a fast Fourier transform with a Hann window function is applied. The signal power is calculated as the root-mean-square (RMS) of the recorded voltage. While this measure does not allow direct comparison of signal power between the ICRF strap and the B-dot probes, it is suitable for tracking temporal evolution on a given detector and comparing the signal strength across different B-dot probes.

III. NATURE OF ICE IN MAXWELLIAN PLASMAS

ICE driven by fast ions was predicted for Wendelstein 7-X in reference[50], where the emission is attributed to the magnetoacoustic ion cyclotron instability. In that case, the signal is detectable both on the B-dot probes and on the ICRF antenna strap. More recently, Kolesnichenko[51] proposed a theory describing the formation of ICE through the interaction of ions from a Maxwellian distribution, without any fast ions, with purely electrostatic fluctuations. This theory was a reaction to the above-mentioned observations from MAST-Upgrade[40].

Figure 2 compares signals collected by the ICRF antenna strap and a B-dot probe during Wendelstein 7-X discharge 20250423.48. This was a purely ECRH-heated plasma, with neutral beam injection (NBI) blips added for diagnostic purposes. A clear ICE signature is observed on the ICRF strap throughout most of the discharge. When NBI is applied after t = 4 s, fast-ion-induced ICE (also referred to as NBI-induced ICE) appears and is superimposed on the pre-existing TPICE in the ICRF strap signal. Importantly, the fast-ion-induced ICE is also clearly visible on the B-dot probe. This is consistent with results from DIII-D, where full-wave simulations demonstrated that NBI-driven ICE can propagate across the plasma-wall gap and be detected as a fast electromagnetic wave[52].

In contrast, TPICE - although similar in power to the NBI-induced ICE - is entirely absent on the B-dot probe. According to ICRF strap measurements (Figure 2(C)), the NBI-induced signal is only about four times stronger than TPICE. Given that the B-dot probe reliably detects the fast-ion-induced signal, the absence of a TPICE signature on the same probe suggests that the Maxwellian emission lacks a substantial magnetic component. This supports the hypothesis that TPICE is predominantly electrostatic in nature.

Importantly, this observation differs from the observations from TUMAN-3M[42], where the emission from the plasma in absence of NBI was detected by the magnetic probes.

Since the measurements are performed at different toroidal locations, where plasma cross-sections and the magnetic field topologies are different, we cannot completely exclude the spatial effect, although it is unlikely since the observations are consistent though all the magnetic field configurations which we tried in the last experimental campaign.

IV. ICE AT DIFFERENT STAGES OF A DISCHARGE.

Quasi–steady-state emission on harmonics of the ion cyclotron frequency is regularly observed in W7-X during the developed phase of the discharge. The frequency and power of this emission depend on the working gas, electron temperature and density, and the magnetic configuration in use. A so-called cleaning discharge, 20250306.34, carried out in the standard configuration (EIM), is shown in Fig. 3. These discharges are typically used to regain density control after high-density experiments when subsequent experiments require low or moderate densities. In such cases, the target density is set intentionally low—practically unreachable—and the plasma is sustained by recycled gas from the vessel walls,

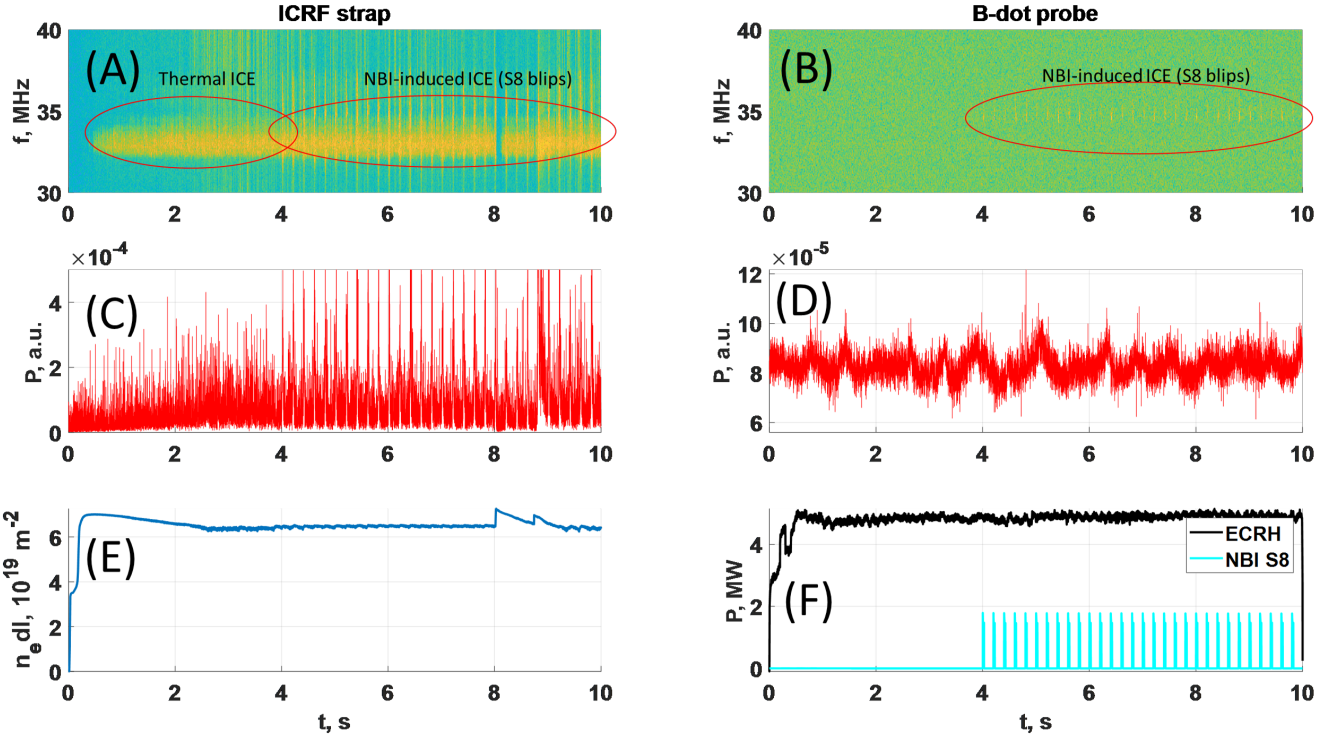

FIG. 2. Wendelstein 7-X discharge 20250423.48. (A) Spectrogram of the ICE signal from the ICRF antenna strap after 10 dB attenuation (log scale); (B) Spectrogram of the ICE signal from the B-dot probe after 25 dB amplification; (C) Power of the attenuated signal collected from the ICRF strap; (D) Power of the amplified signal collected from the B-dot probe; (E) Time trace of line-integrated electron density; (F) Heating power trace during the discharge.

thereby helping to unload them. The heating power is provided by 1.5 MW of central X2 ECRH (gyrotrons D1 and D5 at fixed settings) and kept constant for reproducibility. A well-executed cleaning discharge typically ends due to a density interlock.

The upper panel of Fig. 3 presents a spectrogram of the ICRF strap signal, where the intensity of the emission lines steadily increases as the plasma density decreases and the temperature difference between electrons and ions grows.

The first ICE harmonic, initially faint, becomes clearly visible at around 11 s. As the temperature drops, higher harmonics begin to appear. At even lower densities, we observe a sharp increase in ICE power, the emergence of a broadband feature around 14 MHz, and the eventual disappearance of harmonics into a broadband signal. It is unclear whether this broadband feature is truly physical or an artifact of receiver saturation; however, in the later stages of the discharge, we see an exponential increase in signal power without any indication of detector saturation.

This phenomenon is illustrated in Fig. 4, which shows the plasma stored energy as a function of the line-integrated density. The plot reveals multiple transport regimes, with $W_{\mathrm{dia}} \propto \tau_E$ under conditions of constant heating power and deposition. A non-monotonic trend is evident, suggesting a degradation of plasma energy confinement with increasing density over a certain range.

Just before the exponential increase in ICE power, a mode appears at 15 MHz. As shown by the blue markers in figure 4, the response of W_{dia} to increasing density is weaker than during the earlier stages of the discharge. A linear regression shows that the slopes of $W_{dia}(n_e)$ differ significantly between these two regimes: $117{\cdot}10^{-19}\ kJ \cdot m^2$ (red squares) vs. $74{\cdot}10^{-19}\ kJ \cdot m^2$ (blue circles). Given a steady decrease of radiated power in the discharge towards lower densities, it indicates that energy transport becomes more efficient at low density.

Figure 5 (top panel) shows 100 ms-averaged power spectra at different times during the discharge, normalized to the spectrum at $t = 15$ s. Initially, the signal shows modest growth, followed by a sudden increase in power below 200 MHz. During this phase, harmonics vanish and are replaced by a strong broadband emission. The middle panel shows the maximum ADC voltage recorded in each 20 μs segment, indicating that saturation begins only at $t = 28.6$ s, well after the broadband signal becomes apparent. Thus, the broadband character is not a result of detector saturation.

The nature of this broadband ICE is still unclear. However, it is the only fluctuation-related signal that increases significantly in power during the phase associated with enhanced transport, as shown in the blue region of figure 4.

Although the power spectral density (PSD) of the broadband signal in the 10–200 MHz range exceeds that at $t = 15$ s

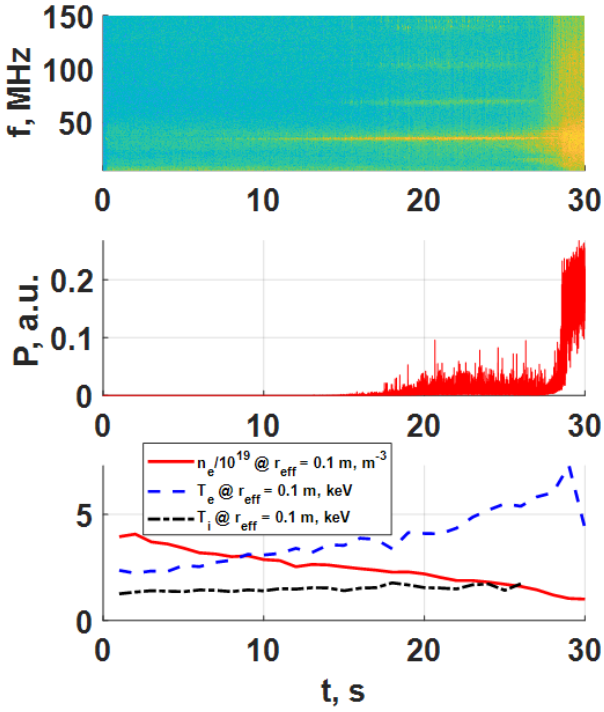

FIG. 3. W7-X hydrogen discharge 20250306.34. The upper panel shows the ICE spectrogram, followed by the relative signal power. Plasma parameters near the core are shown in the lower panel.

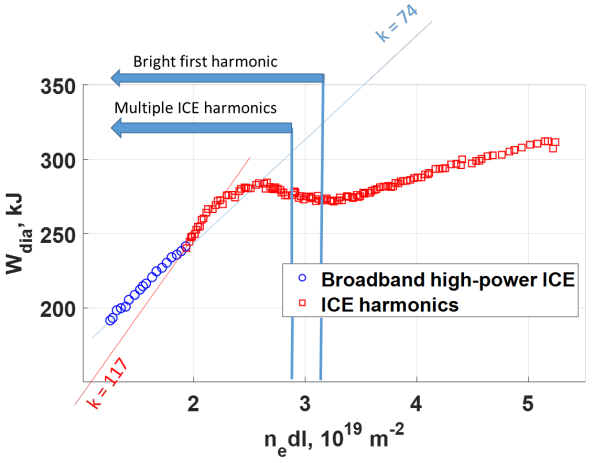

FIG. 4. Diamagnetic energy as a function of line-integrated electron density. The region marked in red corresponds to regular ICE harmonics ($n_{e,dl} < 2.9 \cdot 10^{19}$ m^{-2}). The blue section indicates the regime with exponential growth in ICE power.

by factors of 10–10^4, the harmonics themselves do not show a comparable increase. Most of the broadband power lies between 25 and 50 MHz. The main peak shifts to higher frequencies, and the signal becomes modulated by harmonics of two components around 700–800 kHz. A weaker version of this modulation is already visible at $t = 15$ s. We observe similar modulation patterns in simulations (see section V).

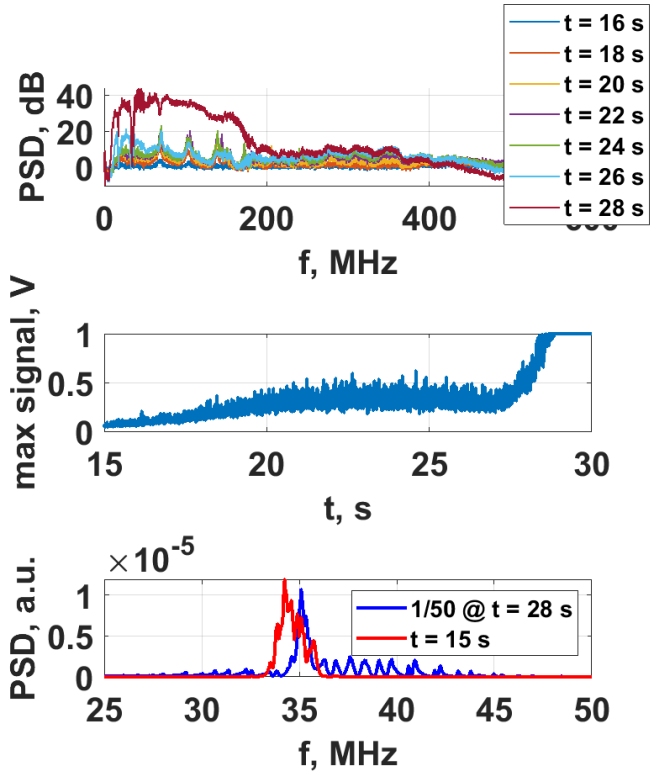

FIG. 5. W7-X hydrogen discharge 20250306.34. Top: Average power spectra (100 ms) at different times, relative to $t = 15$ s. Middle: Maximum ADC voltage during each 20 μs acquisition, showing signal saturation beginning at $t = 28.6$s. Bottom: PSDs at $t = 15$ s and $t = 28$ s, the latter scaled by 1/50.

V. INTERPRETATION OF THE ICE SIGNAL

Ion cyclotron emission is usually generated near the last closed flux surface (LCFS), close to the receiving antenna. In Wendelstein 7-X, this appears to be the case as well. Due to the stellarator's three-dimensional magnetic geometry, edge profiles vary poloidally and toroidally. Nevertheless, reliable profile measurements exist for electron temperature, electron density, and ion temperature all the way up to the separatrix inside the LCFS.

In this study, we use the theoretical model proposed by Kolesnichenko et al.[51], where TPICE is generated through the interaction of electrostatic fluctuations with ions from the Maxwellian tail whose velocities slightly exceed the thermal value, as well as by excitation of ion cyclotron waves.

The growth rate of the instability and the corresponding frequency shift from the ion cyclotron frequency for the case of interaction with the electrostic waves are given by:

$$\gamma = -\omega \hat{I}_l \tau_{ei} \frac{\sigma_{0e}}{\tau_{ei}^2 (1-\hat{I}_0)^2 + \sigma_{0e}^2} \tag{1}$$

$$\Delta\omega = \omega \hat{I}_l \tau_{ei} \frac{\tau_{ei}(1-\hat{I}_0)}{\tau_{ei}^2 (1-\hat{I}_0)^2 + \sigma_{0e}^2} \tag{2}$$

$$\sigma_{0e} = \sqrt{\pi} |x_{0e}| e^{-x_{0e}^2} \left(1 + \tau_{ei} k_\perp \rho_i^2 \frac{\omega_{ci}}{\omega} \left(\frac{n_e'}{n_e} + (x_{0e}^2 - 0.5)\frac{T_e'}{T_e}\right)\right) \tag{3}$$

Here:

- $\omega = l\omega_{ci} + \Delta\omega$ is the angular frequency of the emission,
- ω_{ci} is the ion cyclotron frequency,
- $\hat{I}_l$ and $\hat{I}_0$ are modified Bessel functions of the l^{th} and 0^{th} order evaluated at $k_\perp^2 \rho_i^2$,
- $x_{0e} = \omega/(k_\parallel v_{Te})$,
- ρ_i is the ion gyroradius,
- $k_\perp$ is the perpendicular wavenumber,
- $\tau_{ei} = T_e/T_i$,
- n_e'/n_e and T_e'/T_e are the normalized radial gradients of electron density and temperature, respectively. Particularly, it shows that temperature and density gradients are sources of free energy for the instability.

The frequency shift and the growth rate originating from interaction with ordinary cyclotron waves is given by:

$$\Delta\omega = -\frac{\omega_{ci} M_e \hat{I}_l \omega_{pe}^2}{M_i(\omega_{pe}^2 + c^2 k^2)} \tag{4}$$

$$\gamma = 2\sqrt{\pi} |x_{li}^3| e^{-x_{li}^2} \Delta\omega \times \left(1 - \frac{k_\perp \rho_i}{l}\left(\frac{n_i'}{n_i} + \frac{T_i'}{T_i}\left(x_{li}^2 - 0.5 + z_i \frac{\hat{I}_l'}{\hat{I}_l}\right)\right)\right), \tag{5}$$

Here:

- $x_{li} = \frac{\omega - l\omega_{ci}}{k_\parallel T_i}$,
- ω_{pe} is electron plasma frequency
- $x_{li} = \frac{\omega - l\omega_{ci}}{k_\parallel v_{ti}}$.

Due to the unknown localization of the emission source, the stability analysis was performed across a scan of toroidal angles and radii at the outer mid-plane of Wendelstein 7-X. The simulated spectrum is constructed as a histogram of growth rates for which $\gamma > 10\,\text{s}^{-1}$, plotted as a function of frequency $f = (\omega_{ci} + \Delta\omega)/2\pi$. The perpendicular wavevector was scanned from $k_\perp = 2000$ to $8000\,\text{m}^{-1}$, and $k_\parallel < 10\,\text{m}^{-1}$.

Figure 6 compares the normalized simulated spectrum with the measured one. The simulation begins at 35 MHz, which corresponds to the minimum ion cyclotron frequency at the LCFS on the outer mid-plane. In both cases, the unstable region is located in the outer half of the minor radius.

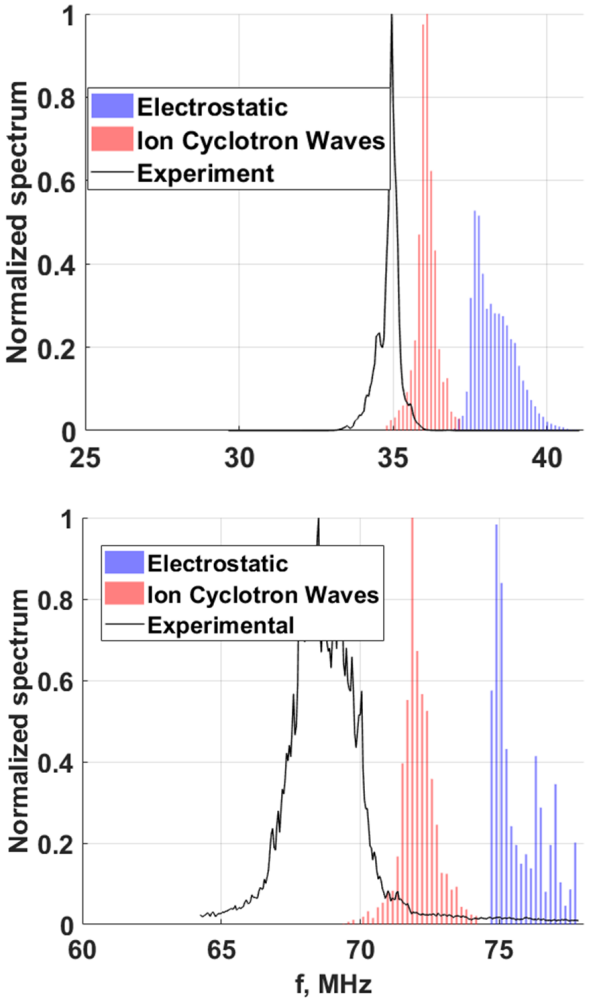

FIG. 6. W7-X experiment 20250306.34 @ t = 20 s. Simulated spectrum (blue bars for simulated ICE from electrostatic fluctuations, red bars for destabilized ordinary cyclotron waves) overlaid with the measured ICE spectrum for the first (upper panel) and the second (lower panel) ICE harmonics.

When the excitation is driven by electrostatic fluctuations, the instability appears with a frequency offset of about 2–5 MHz above the cyclotron frequency. If the excitation is instead due to amplification of ordinary cyclotron waves, the offset is much smaller, less than 0.1 MHz—and it can be either positive or negative. Since ion cyclotron waves are electromagnetic and no TPICE is observed in the B-dot probe signal, we believe that TPICE is unlikely to be caused by ion cyclotron waves, even though the simulations suggest they can become unstable.

The simulation only reproduces the tail of the emission distribution, while the actual maximum lies at 34.25 MHz and is orders of magnitude stronger than in the tail. This suggests that the main source of TPICE is located outside the LCFS, in a region that cannot be modeled with the available experimen-

tal data.

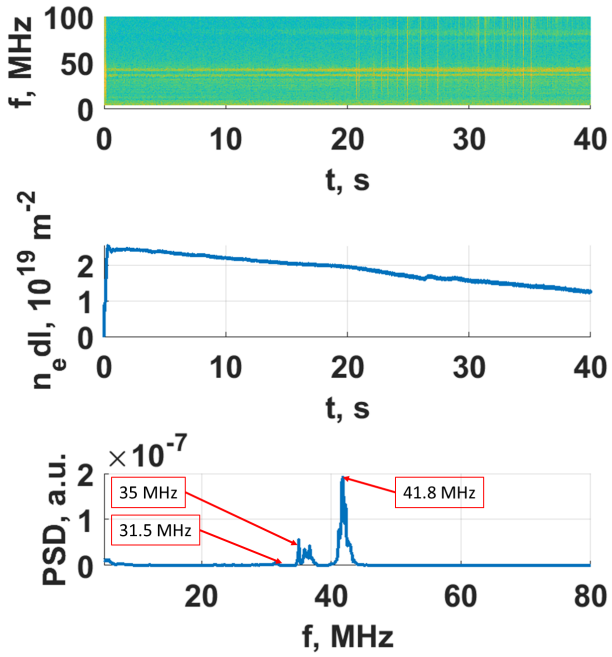

FIG. 7. TPICE signal in helium discharge 20250507.74. Top: spectrogram (log scale); Middle: time trace of ICE signal power; Bottom: ICE spectrum at $t = 15\,\mathrm{s}$.

Helium discharges exhibit a completely different behavior. Figure 7 presents results from discharge 20250507.74 in helium-4, performed in the reversed mirror (XIM) configuration, where the coil currents in the bean-shaped cross-section exceed those in the triangular cross-section.

In this discharge, the fundamental cyclotron harmonic is completely absent. Only a weak feature is visible at approximately 35–36 MHz, which could correspond to the second harmonic. The dominant spectral peak appears at 41.8 MHz, which does not correspond to any ion cyclotron harmonic. This feature is seen in both helium and hydrogen discharges in the XIM configuration, suggesting a magnetic configuration effect rather than an isotope effect.

The theory by Kolesnichenko requires emission to occur predominantly at the fundamental harmonic. This condition is not satisfied in helium discharges at Wendelstein 7-X, and the theory therefore appears to be inapplicable in this case.

Colloquially, the parametric decay instability (PDI) of the gyrotron beam[53–56] was also considered a possible cause of the observed instability. This type of instability was previously observed in Wendelstein 7-X[57] when a powerful gyrotron beam intersected a divertor island. The decay cascade of the gyrotron beam proceeds as follows: the extraordinary-polarized pump wave (i.e., the gyrotron beam) transfers its energy to two upper hybrid (UH) waves trapped in the island, which in turn decay into a cascade of ion Bernstein waves (IBWs). The final stage of this decay, involving the generation of IBWs, raises suspicion that this might indeed be the mechanism behind the observed signal.

However, for the initial decay of the pump wave into UH waves to occur, a specific condition must be met: the sum of the frequencies of the two trapped UH waves must equal the frequency of the pump wave, and the UH frequencies must both lie near 70 GHz. In Wendelstein 7-X, this condition is only transiently satisfied, typically early in the discharge, and requires a specially developed plasma scenario.

In contrast, TPICE is regularly observed over a broad range of densities and temperatures. Therefore, it is unlikely that PDI is responsible for the observed TPICE signal.

VI. CONCLUSIONS

In this paper, we investigated TPICE in Wendelstein 7-X, with particular emphasis on its detection, spectral characteristics, and theoretical interpretation.

Our key findings are summarized as follows:

- TPICE is consistently detected only on the strap of the ICRF antenna, which is sensitive to both magnetic and electrostatic components of plasma fluctuations. In contrast, the B-dot probes, which detect only magnetic fluctuations, do not observe TPICE, indicating that electrostatic effects may play a significant role in its generation.
- We observe that TPICE evolves differently across transport regimes. At low electron densities in standard magnetic configuration, the ICE signal exhibits an exponential growth in power, ultimately saturating the ADC. This phase correlates with a transition to a degraded confinement regime, even though no significant low-frequency plasma activity is observed, suggesting a possible (though not proven) link between ICE and transport processes.
- The ICE spectrum often exhibits multiple local maxima, separated by approximately 700–800 kHz.
- The theoretical model proposed by Kolesnichenko can only be tested for the plasma inside the LCFS. There, the simulations predict instabilities driven by both the interaction of thermal ions with electrostatic fluctuations and with ordinary cyclotron waves. However, the predicted frequency range for these instabilities is much higher than what is observed, indicating that the actual source of the instability may lie at the plasma edge, where modeling is not feasible.
- Discharges in helium cannot be studied with Kolesnichenko's theory, since no ICE at the fundamental frequency is observed.

In conclusion, TPICE in Wendelstein 7-X reveals rich diagnostic and physical information about the edge

plasma and underlying microinstabilities. While the theory of Kolesnichenko provides a promising insights in certain regimes, further theoretical and experimental work—particularly in helium plasmas and varied magnetic configurations—is required to fully understand the origins and implications of TPICE.

ACKNOWLEDGEMENTS

This work has been carried out within the framework of the EUROfusion Consortium, funded by the European Union via the Euratom Research and Training Programme (Grant Agreement No 101052200 — EUROfusion). Views and opinions expressed are however those of the author(s) only and do not necessarily reflect those of the European Union or the European Commission. Neither the European Union nor the European Commission can be held responsible for them.

[1] S. Cauffman and R. Majeski, "Ion cyclotron emission on the tokamak fusion test reactor," Review of Scientific Instruments **66**, 817–819 (1995).

[2] S. Cauffman, R. Majeski, K. G. McClements, and R. O. Dendy, "Alfvenic behaviour of alpha particle driven ion cyclotron emission in tftr," Nuclear Fusion **35**, 1597–1602 (1995).

[3] G. A. Cottrell and R. O. Dendy, "Superthermal radiation from fusion products in jet," Physical Review Letters **60**, 33–36 (1988).

[4] G. A. Cottrell, V. P. Bhatnagar, O. D. Costa, R. O. Dendy, J. Jacquinot, K. G. McClements, D. C. McCune, M. F. F. Nave, P. Smeulders, and D. F. H. Start, "Ion cyclotron emission measurements during jet deuterium-tritium experiments," Nuclear Fusion **33**, 1365 (1993).

[5] P. Schild, G. A. Cottrell, and R. O. Dendy, "Sawtooth oscillations in ion cyclotron emission from jet," Nuclear Fusion **29**, 834 (1989).

[6] K. G. McClements, C. Hunt, R. O. Dendy, and G. Cottrell, "Ion cyclotron emission from jet d-t plasmas," Physical Review Letters **82**, 2099–2102 (1999).

[7] R. O. Dendy, K. G. McClements, C. N. Lashmore-Davies, G. A. Cottrell, R. Majeski, and S. Cauffman, "Ion cyclotron emission due to collective instability of fusion products and beam ions in tftr and jet," Nuclear Fusion **35**, 1733–1742 (1995).

[8] R. O. Dendy, K. G. McClements, C. N. Lashmore-Davies, R. Majeski, and S. Cauffman, "A mechanism for beam-driven excitation of ion cyclotron harmonic waves in the tokamak fusion test reactor," Physics of Plasmas **1**, 3407–3413 (1994).

[9] K. E. Thome, D. C. Pace, R. I. Pinsker, M. A. V. Zeeland, W. W. Heidbrink, and M. E. Austin, "Central ion cyclotron emission in the diii-d tokamak," Nuclear Fusion **59**, 086011 (2019).

[10] K. E. Thome, D. C. Pace, R. I. Pinsker, O. Meneghini, C. A. del Castillo, and Y. Zhu, "Radio frequency measurements of energetic-particle-driven emission using the ion cyclotron emission diagnostic on the diii-d tokamak," Review of Scientific Instruments **89**, 10I102 (2018).

[11] B. Chapman, R. O. Dendy, S. C. Chapman, K. G. McClements, G. S. Yun, S. G. Thatipamula, and M. H. Kim, "Nonlinear wave interactions generate high-harmonic cyclotron emission from fusion-born protons during a kstar elm crash," Nuclear Fusion **58**, 096027 (2018).

[12] B. Chapman, R. O. Dendy, S. C. Chapman, K. G. McClements, and R. Ochoukov, "Origin of ion cyclotron emission at the proton cyclotron frequency from the core of deuterium plasmas in the asdex-upgrade tokamak," Plasma Physics and Controlled Fusion **62**, 095022 (2020).

[13] B. Chapman, R. O. Dendy, S. C. Chapman, K. G. McClements, G. S. Yun, S. G. Thatipamula, and M. H. Kim, "Interpretation of suprathermal emission at deuteron cyclotron harmonics from deuterium plasmas heated by neutral beam injection in the kstar tokamak," Nuclear Fusion **59**, 106021 (2019).

[14] B. Chapman, R. O. Dendy, K. G. McClements, S. C. Chapman, G. S. Yun, S. G. Thatipamula, and M. H. Kim, "Sub-microsecond temporal evolution of edge density during edge localized modes in kstar tokamak plasmas inferred from ion cyclotron emission," Nuclear Fusion **57**, 124004 (2017).

[15] G. H. DeGrandchamp, J. B. Lestz, M. A. V. Zeeland, X. D. Du, W. W. Heidbrink, K. E. Thome, N. A. Crocker, and R. I. Pinsker, "Mode structure measurements of ion cyclotron emission and sub-cyclotron modes on diii-d," Nuclear Fusion **62**, 106033 (2022).

[16] G. H. DeGrandchamp, K. E. Thome, W. W. Heidbrink, I. Holmes, and R. I. Pinsker, "Upgrades to the ion cyclotron emission diagnostic on the diii-d tokamak," Review of Scientific Instruments **92**, 033543 (2021).

[17] N. A. Crocker, S. X. Tang, K. E. Thome, J. B. Lestz, E. V. Belova, A. Zalzali, R. O. Dendy, W. A. Peebles, K. K. Barada, R. Hong, T. L. Rhodes, G. Wang, L. Zeng, T. A. Carter, G. H. DeGrandchamp, W. W. Heidbrink, and R. I. Pinsker, "Novel internal measurements of ion cyclotron frequency range fast-ion driven modes," Nuclear Fusion **62**, 026023 (2022).

[18] L. Liu, X. Zhang, Y. Zhu, C. Qin, Y. Zhao, S. Yuan, Y. Mao, M. Li, K. Zhang, J. Cheng, L. Ai, and Y. Cheng, "Ion cyclotron emission driven by deuterium neutral beam injection and core fusion reaction ions in east," Nuclear Fusion **60**, 044002 (2020).

[19] L. Liu, R. Ochoukov, K. G. McClements, R. O. Dendy, V. Bobkov, M. Weiland, R. Bilato, H. Faugel, D. Moseev, M. Salewski, W. Zhang, X. Zhang, Y. Zhu, B. Chapman, A. Zalzali, A. U. team, and E. M. team, "Explanation of core ion cyclotron emission from beam-ion heated plasmas in asdex upgrade by the magnetoacoustic cyclotron instability," Nuclear Fusion **61**, 026004 (2021).

[20] L. Liu, R. Tong, X. Zou, H. Chen, Y. Chen, G. Dong, G. Hao, X. He, Y. Han, X. Ji, A. Liang, B. Li, J. Li, Y. Li, L. Liu, Z. Shi, H. Wei, F. Xia, G. Xiao, J. Yin, D. Yu, B. Yuan, Y. Zhu, W. Zhong, M. Xu, and H.-A. team, "Identification of core ion cyclotron instabilities on hl-2a tokamak," Nuclear Fusion **63**, 104004 (2023).

[21] R. Ochoukov, V. Bobkov, H. Faugel, H. Fünfgelder, and J.-M. Noterdaeme, "A new b-dot probe-based diagnostic for amplitude, polarization, and wavenumber measurements of ion cyclotron range-of frequency fields on asdex upgrade," Review of Scientific Instruments **86**, 115112 (2015), doi: 10.1063/1.4935833.

[22] R. Ochoukov, V. Bobkov, B. Chapman, R. Dendy, M. Dunne, H. Faugel, M. García-Muñoz, B. Geiger, P. Hennequin, K. G. McClements, D. Moseev, S. Nielsen, J. Rasmussen, P. Schneider, M. Weiland, and J.-M. Noterdaeme, "Observations of core ion cyclotron emission on asdex upgrade tokamak," Review of Scientific Instruments **89**, 10J101 (2018).

[23] R. Ochoukov, R. Bilato, V. Bobkov, S. C. Chapman, R. Dendy, M. Dreval, H. Faugel, A. Kappatou, Y. Kazakov, M. Mantsinen, K. G. McClements, D. Moseev, S. K. Nielsen, J. M. Noterdaeme, M. Salewski, P. Schneider, and M. Weiland, "High frequency alfvén eigenmodes detected with ion-cyclotron-emission diagnostics during nbi and icrf heated plasmas on the asdex upgrade tokamak," Nuclear Fusion **60**, 126043 (2020).

[24] E. D. Fredrickson, N. N. Gorelenkov, R. E. Bell, A. Diallo, B. P. LeBlanc, M. Podestà, and N. Team, "Emission in the ion cyclotron range of frequencies (ice) on nstx and nstx-u," Physics of Plasmas **26**, 032111 (2019).

[25] E. D. Fredrickson, N. N. Gorelenkov, R. E. Bell, A. Diallo, B. P. LeBlanc, J. Lestz, M. Podestà, and the NSTX team, "Chirping ion cyclotron emission (ice) on nstx-u," Nuclear Fusion **61**, 086007 (2021).

[26] M. Ichimura, H. Higaki, S. Kakimoto, Y. Yamaguchi, K. Nemoto, M. Katano, M. Ishikawa, S. Moriyama, and T. Suzuki, "Observation of spontaneously excited waves in the ion cyclotron frequency range on jt-60u," Nuclear Fusion **48**, 035012 (2008).

[27] S. SATO, M. ICHIMURA, Y. YAMAGUCHI, M. KATANO, Y. IMAI, T. MURAKAMI, Y. MIYAKE, T. YOKOYAMA, S. MORIYAMA, T. KOBAYASHI, A. KOJIMA, K. SHINOHARA, Y. SAKAMOTO, T. WATANABE, H. HOJO, and T. IMAI, "Observation of ion cyclotron emission owing to dd fusion product h ions in jt-60u," Plasma and Fusion Research **5**, S2067–S2067 (2010).

[28] S. Sumida, K. Shinohara, R. Ikezoe, M. Ichimura, M. Sakamoto, M. Hirata, and S. Ide, "Characteristics of fast 3he ion velocity distribution exciting ion cyclotron emission on jt-60u," Plasma Physics and Controlled Fusion **61**, 025014 (2019).

[29] L. G. Askinazi, A. A. Belokurov, D. B. Gin, V. A. Kornev, S. V. Lebedev, A. E. Shevelev, A. S. Tukachinsky, and N. A. Zhubr, "Ion cyclotron emission in nbi-heated plasmas in the tuman-3m tokamak," Nuclear Fusion **58**, 082003 (2018).

[30] L. G. Askinazi, G. I. Abdullina, A. A. Belokurov, V. A. Kornev, S. V. Krikunov, S. V. Lebedev, D. V. Razumenko, A. S. Tukachinsky, and N. A. Zhubr, "Experimental determination of the dispersion relation of plasma ra-

diation at frequencies of the ion cyclotron resonance and its harmonics in tokamak," Technical Physics Letters **47**, 214–217 (2021).

[31]B. C. G. Reman, R. O. Dendy, T. Akiyama, S. C. Chapman, J. W. S. Cook, H. Igami, S. Inagaki, K. Saito, and G. S. Yun, "Interpreting observations of ion cyclotron emission from large helical device plasmas with beam-injected ion populations," Nuclear Fusion **59**, 096013 (2019).

[32]B. C. G. Reman, R. O. Dendy, T. Akiyama, S. C. Chapman, J. W. S. Cook, H. Igami, S. Inagaki, K. Saito, R. Seki, M. H. Kim, S. G. Thatipamula, and G. S. Yun, "Density dependence of ion cyclotron emission from deuterium plasmas in the large helical device," Nuclear Fusion **61**, 066023 (2021).

[33]B. C. G. Reman, R. O. Dendy, H. Igami, T. Akiyama, M. Salewski, S. C. Chapman, J. W. S. Cook, S. Inagaki, K. Saito, R. Seki, M. Toida, M. H. Kim, S. G. Thatipamula, and G. S. Yun, "First observation and interpretation of spontaneous collective radiation from fusion-born ions in a stellarator plasma," Plasma Physics and Controlled Fusion **64**, 085008 (2022).

[34]K. Saito, H. Kasahara, T. Seki, R. Kumazawa, T. Mutoh, T. Watanabe, F. Shimpo, G. Nomura, M. Osakabe, M. Ichimura, H. Higaki, and A. Komori, "Measurement of ion cyclotron emissions by use of icrf heating antennas in lhd," Fusion Engineering and Design **84**, 1676–1679 (2009).

[35]K. Saito, R. Kumazawa, T. Seki, H. Kasahara, G. Nomura, F. Shimpo, H. Igami, M. Isobe, K. Ogawa, K. Toi, M. Osakabe, M. Nishiura, T. Watanabe, S. Yamamoto, M. Ichimura, and T. Mutoh, "Measurement of ion cyclotron emissions by using high-frequency magnetic probes in the lhd," Plasma Science and Technology **15**, 209–212 (2013).

[36]K. Saito, H. Igami, M. Toida, T. Akiyama, S. Kamio, and R. Seki, "Rf wave detection with high-frequency magnetic probes in lhd," Plasma Fusion Res. **13**, 3402043 (2018).

[37]O. Samant, R. O. Dendy, S. C. Chapman, S. K. P. Tripathi, T. Carter, B. V. Compernolle, and J. W. S. Cook, "Physics of beam-driven ion cyclotron emission in the large plasma device," Nuclear Fusion **65**, 066023 (2025).

[38]R. Ochoukov, K. G. McClements, R. Bilato, V. Bobkov, B. Chapman, S. C. Chapman, R. O. Dendy, M. Dreval, H. Faugel, J.-M. Noterdaeme, M. Salewski, M. Weiland, A. U. Team, and E. M. Team, "Interpretation of core ion cyclotron emission driven by sub-alfvénic beam-injected ions via magnetoacoustic cyclotron instability," Nuclear Fusion **59**, 086032 (2019).

[39]K. G. McClements, A. Brisset, B. Chapman, S. C. Chapman, R. O. Dendy, P. Jacquet, V. G. Kiptily, M. Mantsinen, B. C. G. Reman, and J. E. T. Contributors, "Observations and modelling of ion cyclotron emission observed in jet plasmas using a sub-harmonic arc detection system during ion cyclotron resonance heating," Nuclear Fusion **58**, 096020 (2018).

[40]J. F. Rivero-Rodríguez, K. G. McClements, M. Fitzgerald, S. E. Sharapov, M. Cecconello, N. A. Crocker, I. Dolby, M. Dreval, N. Fil, J. Galdón-Quiroga, M. García-Muñoz, S. Blackmore, W. Heidbrink, S. Henderson, A. Jackson, A. Kappatou, D. Keeling, D. Liu, Y. Q. Liu, C. Michael, H. J. C. Oliver, P. Ollus, E. Parr, G. Prechel, T. Rhodes, D. Ryan, P. Shi, M. Vallar, L. Velarde, T. Williams, H. Wong, the EUROfusion Tokamak Exploitation Team, and the MAST-U Team, "Overview of fast particle experiments in the first mast upgrade experimental campaigns," Nuclear Fusion **64**, 086025 (2024).

[41]S. Sumida, K. Shinohara, M. Ichimura, T. Bando, A. Bierwage, T. Kobayashi, H. Yamazaki, S. Moriyama, and S. Ide, "Observation of ion-cyclotron-range-of-frequency wave emission in electron-cyclotron-resonance-heated tokamak plasma," Plasma Physics and Controlled Fusion **65**, 075002 (2023).

[42]S. V. Lebedev, L. G. Askinazi, A. A. Belokurov, D. B. Gin, V. A. Kornev, A. A. Shabelsky, A. E. Shevelev, A. S. Tukachinsky, and N. A. Zhubr, "Observation of ion cyclotron emission from ohmically and nbi heated plasmas in tuman-3m tokamak," EPJ , 03010 (2017).

[43]R. C. Wolf, A. Alonso, S. Äkäslompolo, J. Baldzuhn, M. Beurskens, C. D. Beidler, C. Biedermann, H.-S. Bosch, S. Bozhenkov, R. Brakel, H. Braune, S. Brezinsek, K.-J. Brunner, H. Damm, A. Dinklage, P. Drewelow, F. Effenberg, Y. Feng, O. Ford, G. Fuchert, Y. Gao, J. Geiger, O. Grulke, N. Harder, D. Hartmann, P. Helander, B. Heinemann, M. Hirsch, U. Höfel, C. Hopf, K. Ida, M. Isobe, M. W. Jakubowski, Y. O. Kazakov, C. Killer, T. Klinger, J. Knauer, R. König, M. Krychowiak, A. Langenberg, H. P. Laqua, S. Lazerson, P. McNeely, S. Marsen, N. Marushchenko, R. Nocentini, K. Ogawa, G. Orozco, M. Osakabe, M. Otte, N. Pablant, E. Pasch, A. Pavone, M. Porkolab, A. P. Sitjes, K. Rahbarnia, R. Riedl, N. Rust, E. Scott, J. Schilling, R. Schroeder, T. Stange, A. von Stechow, E. Strumberger, T. S. Pedersen, J. Svensson, H. Thomson, Y. Turkin, L. Vano, T. Wauters, G. Wurden, M. Yoshinuma, M. Zanini, and D. Zhang, "Performance of wendelstein 7-x stellarator plasmas during the first divertor operation phase," Physics of Plasmas **26**, 82504 (2019).

[44]S. A. Bozhenkov, Y. Kazakov, O. P. Ford, M. N. A. Beurskens, J. Alcusón, J. A. Alonso, J. Baldzuhn, C. Brandt, K. J. Brunner, H. Damm, G. Fuchert, J. Geiger, O. Grulke, M. Hirsch, U. Höfel, Z. Huang, J. Knauer, M. Krychowiak, A. Langenberg, H. P. Laqua, S. Lazerson, N. B. Marushchenko, D. Moseev, M. Otte, N. Pablant, E. Pasch, A. Pavone, J. H. E. Proll, K. Rahbarnia, E. R. Scott, H. M. Smith, T. Stange, A. V. Stechow, H. Thomsen, Y. Turkin, G. Wurden, P. Xanthopoulos, D. Zhang, and R. C. Wolf, "High-performance plasmas after pellet injections in wendelstein 7-x," Nuclear Fusion **60**, 66011 (2020).

[45]T. S. Pedersen, I. Abramovic, P. Agostinetti, M. A. Torres, S. Äkäslompolo, J. A. Belloso, P. Aleynikov, K. Aleynikova, M. Alhashimi, A. Ali, N. Allen, A. Alonso, G. Anda, T. Andreeva, C. Angioni, A. Arkhipov, A. Arnold, W. Asad, E. Ascasibar, M.-H. Aumeunier, K. Avramidis, E. Aymerich, S.-G. Baek, J. Bähner, A. Baillod, M. Balden, M. Balden, J. Baldzuhn, S. Ballinger, M. Banduch, S. Bannmann, A. B. Navarro, A. B. Navarro, T. Barbui, C. Beidler, C. Belafdil, A. Bencze, A. Benndorf, M. Beurskens, C. Biedermann, O. Biletskyi, B. Blackwell, M. Blatzheim, T. Bluhm, D. Böckenhoff, G. Bongiovi, M. Borchardt, D. Borodin, J. Boscary, H. Bosch, T. Bosmann, B. Böswirth, L. Böttger, A. Bottino, S. Bozhenkov, R. Brakel, C. Brandt, T. Bräuer, H. Braune, S. Brezinsek, K. Brunner, S. Buller, R. Burhenn, R. Bussiahn, B. Buttenschön, A. Buzás, V. Bykov, I. Calvo, K. C. Mata, I. Caminal, B. Cannas, A. Cappa, A. Carls, F. Carovani, M. Carr, D. Carralero, B. Carvalho, J. Casas, D. Castano-Bardawil, F. Castejon, N. Chaudhary, I. Chelis, A. Chomiczewska, J. W. Coenen, M. Cole, F. Cordella, Y. Corre, K. Crombe, G. Cseh, B. Csillag, H. Damm, C. Day, M. de Baar, E. D. la Cal, S. Degenkolbe, A. Demby, S. Denk, C. Dhard, A. D. Siena, A. Dinklage, T. Dittmar, M. Dreval, M. Drevlak, P. Drewelow, P. Drews, D. Dunai, E. Edlund, F. Effenberg, G. Ehrke, M. Endler, D. A. Ennis, F. J. Escoto, T. Estrada, E. Fable, N. Fahrenkamp, A. Fanni, J. Faustin, J. Fellinger, Y. Feng, W. Figacz, E. Flom, O. Ford, T. Fornal, H. Frerichs, S. Freundt, G. Fuchert, M. Fukuyama, F. Füllenbach, G. Gantenbein, Y. Gao, K. Garcia, J. M. G. Regaña, I. García-Cortés, J. Gaspar, D. A. Gates, J. Geiger, B. Geiger, L. Giudicotti, A. González, A. Goriaev, D. Gradic, M. Grahl, J. P. Graves, J. Green, E. Grelier, H. Greuner, S. Groß, H. Grote, M. Groth, M. Gruca, O. Grulke, M. Grün, J. G. Arnaiz, S. Günter, V. Haak, M. Haas, P. Hacker, A. Hakola, A. Hallenbert, K. Hammond, X. Han, S. K. Hansen, J. H. Harris, H. Hartfuß, D. Hartmann, D. Hathiramani, R. Hatzky, J. Hawke, S. Hegedus, B. Hein, B. Heinemann, P. Helander, S. Henneberg, U. Hergenhahn, C. Hidalgo, F. Hindenlang, M. Hirsch, U. Höfel, K. P. Hollfeld, A. Holtz, D. Hopf, D. Höschen, M. Houry, J. Howard, X. Huang, M. Hubeny, S. Hudson, K. Ida, Y. Igitkhanov, V. Igochine, S. Illy, C. Ionita-Schrittwieser, M. Isobe, M. Jabłczyńska, S. Jablonski, B. Jagielski, M. Jakubowski, A. J. van Vuuren, J. Jelonnek, F. Jenko, F. Jenko, T. Jensen, H. Jenzsch, P. Junghanns, J. Kaczmarczyk, J. Kallmeyer, U. Kamionka, M. Kandler, S. Kasilov, Y. Kazakov, D. Kennedy, A. Kharwandikar, M. Khokhlov, C. Kiefer, C. Killer, A. Kirschner, R. Kleiber, T. Klinger, S. Klose, J. Knauer, A. Knieps, F. Köchl, G. Kocsis, Y. Kolesnichenko, A. Könies, R. König, J. Kontula, P. Kornejew, J. Koschinsky, M. M. Kozulia, A. Krämer-Flecken, R. Krampitz, M. Krause, N. Krawczyk, T. Kremeyer, L. Krier, D. M. Kriete, M. Krychowiak, I. Ksiazek, M. Kubkowska, M. Kuczynski, G. Kühner, A. Kumar, T. Kurki-Suonio, S. Kwak, M. Landreman, P. T. Lang, A. Langenberg, H. P. Laqua, H. Laqua, R. Laube, S. Lazerson, M. Lewerentz, C. Li, Y. Liang, C. Linsmeier, J. Lion, A. Litnovsky, S. Liu, J. Lobsien, J. Loizu, J. Lore, A. Lorenz, U. Losada, F. Louche, R. Lunsford, V. Lutsenko, M. Machielsen, F. Mackel, J. Maisano-Brown, O. Maj, D. Makowski, G. Manduchi, E. Maragkoudakis, O. Marchuk, S. Marsen, E. Martines, J. Martinez-Fernandez, M. Marushchenko, S. Masuzaki, D. Maurer, M. Mayer, K. J. McCarthy, O. Mccormack, P. McNeely, H. Meister, B. Mendelevitch, S. Mendes, A. Merlo, A. Messian, A. Mielczarek, O. Mishchenko, B. Missal, R. Mitteau, V. E. Moiseenko, A. Mollen, V. Moncada, T. Mönnich, T. Morisaki, D. Moseev, G. Motojima, S. Mulas, M. Mulsow, M. Nagel, D. Naujoks, V. Naulin, T. Neelis, H. Neilson, R. Neu, O. Neubauer, U. Neuner, D. Nicolai, S. K. Nielsen, H. Niemann, T. Nishiza, T. Nishizawa, T. Nishizawa, C. Nührenberg, R. Ochoukov, J. Oelmann, G. Offermanns, K. Ogawa, S. Okamura, J. Ölmanns, J. On-

gena, J. Oosterbeek, M. Otte, N. Pablant, N. P. Alvarez, N. P. Alvarez, A. Pandey, E. Pasch, R. Pavlichenko, A. Pavone, E. Pawelec, G. Pechstein, G. Pelka, V. Perseo, B. Peterson, D. Pilopp, S. Pingel, F. Pisano, B. Plöckl, G. Plunk, P. Pölöskei, B. Pompe, A. Popov, M. Porkolab, J. Proll, M. J. Pueschel, M.-E. Puiatti, A. P. Sitjes, F. Purps, K. Rahbarnia, M. Rasiński, J. Rasmussen, A. Reiman, F. Reimold, M. Reisner, D. Reiter, M. Richou, R. Riedl, J. Riemann, K. Rieße, G. Roberg-Clark, V. Rohde, J. Romazanov, D. Rondeshagen, P. Rong, L. Rudischhauser, T. Rummel, K. Rummel, A. Runov, N. Rust, L. Ryc, P. Salembier, M. Salewski, E. Sanchez, S. Satake, G. Satheeswaran, J. Schacht, E. Scharff, F. Schauer, J. Schilling, G. Schlisio, K. Schmid, J. Schmitt, O. Schmitz, W. Schneider, M. Schneider, P. Schneider, R. Schrittwieser, T. Schröder, M. Schröder, R. Schroeder, B. Schweer, D. Schwörer, E. Scott, E. Scott, B. Shanahan, G. Sias, P. Sichta, M. Singer, P. Sinha, S. Sipliä, C. Slaby, M. Sleczka, H. Smith, J. Smoniewski, E. Sonnendrücker, M. Spolaore, A. Spring, R. Stadler, D. Stańczak, T. Stange, I. Stepanov, L. Stephey, J. Stober, U. Stroth, E. Strumberger, C. Suzuki, Y. Suzuki, J. Svensson, T. Szabolics, T. Szepesi, M. Szücs, F. L. Tabarés, N. Tamura, A. Tancetti, C. Tantos, J. Terry, H. Thienpondt, H. Thomsen, M. Thumm, J. M. Travere, P. Traverso, J. Tretter, E. Trier, H. T. Mora, T. Tsujimura, Y. Turkin, A. Tykhyi, B. Unterberg, P. van Eeten, B. van Milligen, M. van Schoor, L. Vano, S. Varoutis, M. Vecsei, L. Vela, J. L. Velasco, M. Vervier, N. Vianello, H. Viebke, R. Vilbrandt, G. Vogel, N. Vogt, C. Volkhausen, A. von Stechow, F. Wagner, E. Wang, H. Wang, F. Warmer, T. Wauters, L. Wegener, T. Wegner, G. Weir, U. Wenzel, A. White, F. Wilde, F. Wilms, T. Windisch, M. Winkler, A. Winter, V. Winters, R. Wolf, A. M. Wright, G. A. Wurden, P. Xanthopoulos, S. Xu, H. Yamada, H. Yamaguchi, M. Yokoyama, M. Yoshinuma, Q. Yu, M. Zamanov, M. Zanini, M. Zarnstorff, D. Zhang, S. Zhou, J. Zhu, C. Zhu, M. Zilker, A. Zocco, H. Zohm, S. Zoletnik, and L. Zsuga, "Experimental confirmation of efficient island divertor operation and successful neoclassical transport optimization in wendelstein 7-x," Nuclear Fusion **62**, 042022 (2022).

[46]T. Klinger, C. Baylard, C. D. Beidler, J. Boscary, H. S. Bosch, A. Dinklage, D. Hartmann, P. Helander, H. Maßberg, A. Peacock, T. S. Pedersen, T. Rummel, F. Schauer, L. Wegener, and R. Wolf, "Towards assembly completion and preparation of experimental campaigns of wendelstein 7-x in the perspective of a path to a stellarator fusion power plant," Fusion Engineering and Design **88**, 461–465 (2013).

[47]A. Dinklage, C. D. Beidler, P. Helander, G. Fuchert, H. Maaßberg, K. Rahbarnia, T. S. Pedersen, Y. Turkin, R. C. Wolf, A. Alonso, T. Andreeva, B. Blackwell, S. Bozhenkov, B. Buttenschön, A. Czarnecka, F. Effenberg, Y. Feng, J. Geiger, M. Hirsch, U. Höfel, M. Jakubowski, T. Klinger, J. Knauer, G. Kocsis, A. Krämer-Flecken, M. Kubkowska, A. Langenberg, H. P. Laqua, N. Marushchenko, A. Mollén, U. Neuner, H. Niemann, E. Pasch, N. Pablant, L. Rudischhauser, H. M. Smith, O. Schmitz, T. Stange, T. Szepesi, G. Weir, T. Windisch, G. A. Wurden, D. Zhang, I. Abramovic, S. Äkäslompolo, A. Ali, A. Alonso, J. A. Belloso, P. Aleynikov, K. Aleynikova, R. Alzbutas, G. Anda, T. Andreeva, E. Ascasibar, J. Assmann, S.-G. Baek, J. Baldzuhn, M. Banduch, T. Barbui, M. Barlak, K. Baumann, W. Behr, C. Beidler, A. Benndorf, O. Bertuch, M. Beurskens, C. Biedermann, W. Biel, D. Birus, B. Blackwell, E. Blanco, M. Blatzheim, T. Bluhm, D. Böckenhoff, P. Bolgert, M. Borchardt, V. Borsuk, J. Boscary, H.-S. Bosch, L.-G. Böttger, S. Bozhenkov, R. Brakel, H. Brand, C. Brandt, T. Bräuer, H. Braune, S. Brezinsek, K.-J. Brunner, B. Brünner, R. Burhenn, R. Bussiahn, B. Buttenschön, V. Bykov, Y. Cai, I. Calvo, B. Cannas, A. Cappa, A. Card, A. Carls, L. Carraro, B. Carvalho, F. Castejon, A. Charl, F. Chernyshev, M. Cianciosa, R. Citarella, Ciupiński, G. Claps, M. J. Cole, F. Cordella, G. Cseh, A. Czarnecka, A. Czermak, K. Czerski, M. Czerwinski, G. Czymek, A. da Molin, A. da Silva, G. Dammertz, A. de la Pena, S. Degenkolbe, P. Denner, A. Dinklage, T. Dittmar, C. P. Dhard, M. Dostal, M. Drevlak, P. Drewelow, P. Drews, A. Dudek, G. Dundulis, F. Durodie, P. van Eeten, F. Effenberg, G. Ehrke, M. Endler, D. Ennis, E. Erckmann, H. Esteban, T. Estrada, N. Fahrenkamp, J.-H. Feist, J. Fellinger, Y. Feng, H. Fernandes, W. H. Fietz, W. Figacz, J. Fontdecaba, O. Ford, T. Fornal, H. Frerichs, A. Freund, G. Fuchert, M. Führer, T. Funaba, A. Galkowski, G. Gantenbein, Y. Gao, J. G. Regaña, M. Garcia-Munoz, D. Gates, G. Gawlik, B. Geiger, J. Geiger, V. Giannella, N. Gierse, A. Gogoleva, B. Goncalves, A. Goriaev, D. Gradic, M. Grahl, J. Green, A. Grosman, H. Grote, M. Gruca, O. Grulke, C. Guerard, P. Hacker, L. Haiduk, K. Hammond, X. Han, F. Harberts, J. H. Harris, H.-J. Hartfuß, D. Hartmann, D. Hathiramani, B. Hein, B. Heinemann, P. Heitzenroeder, S. Henneberg, P. Helander, C. Hennig, J. H. Sanchez, C. Hidalgo, M. Hirsch, U. Höfel, H. Hölbe, K. P. Hollfeld, A. Hölting, D. Höschen, M. Houry, J. Howard, X. Huang, M. Huber, V. Huber, H. Hunger, K. Ida, T. Ilkei, S. Illy, B. Israeli, A. Ivanov, S. Jablonski, J. Jagielski, M. Jakubowski, J. Jelonnek, H. Jenzsch, P. Junghans, J. Kacmarczyk, T. Kaliatka, J.-P. Kallmeyer, U. Kamionka, R. Karalevicius, H. Kasahara, W. Kasparek, Y. Kazakov, N. Kenmochi, M. Keunecke, A. Khilchenko, C. Killer, D. Kinna, R. Kleiber, T. Klinger, J. Knauer, M. Knaup, A. Knieps, T. Kobarg, G. Kocsis, F. Köchl, Y. Kolesnichenko, A. Könies, M. Köppen, J. Koshurinov, R. Koslowski, R. König, F. Köster, P. Kornejew, R. Koziol, M. Krämer, A. Krämer-Flecken, R. Krampitz, P. Kraszewsk, N. Krawczyk, T. Kremeyer, T. Krings, J. Krom, M. Krychowiak, G. Krzesinski, I. Ksiazek, M. Kubkowska, G. Kühner, T. Kurki-Suonio, S. Kwak, M. Landreman, R. Lang, A. Langenberg, S. Langish, H. Laqua, H. P. Laqua, R. Laube, S. Lazerson, C. Lechte, M. Lennartz, W. Leonhardt, L. Lewerentz, Y. Liang, C. Linsmeier, S. Liu, J.-F. Lobsien, D. Loesser, J. L. Cisquella, J. Lore, A. Lorenz, M. Losert, L. Lubyako, A. Lücke, A. Lumsdaine, V. Lutsenko, H. Maaßberg, J. Maisano-Brown, O. Marchuk, M. Mardenfeld, P. Marek, S. Marsen, M. Marushchenko, S. Masuzaki, D. Maurer, K. McCarthy, P. McNeely, A. Meier, , and the W7-X Team, "Publisher correction: Magnetic configuration effects on the wendelstein 7-x stellarator," Nature Physics **14**, 867 (2018).

[48]C. D. Beidler, H. M. Smith, A. Alonso, T. Andreeva, J. Baldzuhn, M. N. A. Beurskens, M. Borchardt, S. A. Bozhenkov, K. J. Brunner, H. Damm, M. Drevlak, O. P. Ford, G. Fuchert, J. Geiger, P. Helander, U. Hergenhahn, M. Hirsch, U. Höfel, Y. O. Kazakov, R. Kleiber, M. Krychowiak, S. Kwak, A. Langenberg, H. P. Laqua, U. Neuner, N. A. Pablant, E. Pasch, A. Pavone, T. S. Pedersen, K. Rahbarnia, J. Schilling, E. R. Scott, T. Stange, J. Svensson, H. Thomsen, Y. Turkin, F. Warmer, R. C. Wolf, D. Zhang, I. Abramovic, S. Äkäslompolo, J. Alcusón, P. Aleynikov, K. Aleynikova, A. Ali, A. Alonso, G. Anda, E. Ascasibar, J. P. Bähner, S. G. Baek, M. Balden, M. Banduch, T. Barbui, W. Behr, A. Benndorf, C. Biedermann, W. Biel, B. Blackwell, E. Blanco, M. Blatzheim, S. Ballinger, T. Bluhm, D. Böckenhoff, B. Böswirth, L.-G. Böttger, V. Borsuk, J. Boscary, H.-S. Bosch, R. Brakel, H. Brand, C. Brandt, T. Bräuer, H. Braune, S. Brezinsek, K.-J. Brunner, R. Burhenn, R. Bussiahn, B. Buttenschön, V. Bykov, J. Cai, I. Calvo, B. Cannas, A. Cappa, A. Carls, L. Carraro, B. Carvalho, F. Castejon, A. Charl, N. Chaudhary, D. Chauvin, F. Chernyshev, M. Cianciosa, R. Citarella, G. Claps, J. Coenen, M. Cole, M. J. Cole, F. Cordella, G. Cseh, A. Czarnecka, K. Czerski, M. Czerwinski, G. Czymek, A. da Molin, A. da Silva, A. de la Pena, S. Degenkolbe, C. P. Dhard, M. Dibon, A. Dinklage, T. Dittmar, P. Drewelow, P. Drews, F. Durodie, E. Edlund, F. Effenberg, G. Ehrke, S. Elgeti, M. Endler, D. Ennis, H. Esteban, T. Estrada, J. Fellinger, Y. Feng, E. Flom, H. Fernandes, W. H. Fietz, W. Figacz, J. Fontdecaba, T. Fornal, H. Frerichs, A. Freund, T. Funaba, A. Galkowski, G. Gantenbein, Y. Gao, J. G. Regaña, D. Gates, B. Geiger, V. Giannella, A. Gogoleva, B. Goncalves, A. Goriaev, D. Gradic, M. Grahl, J. Green, H. Greuner, A. Grosman, H. Grote, M. Gruca, O. Grulke, C. Guerard, P. Hacker, X. Han, J. H. Harris, D. Hartmann, D. Hathiramani, B. Hein, B. Heinemann, P. Helander, S. Henneberg, M. Henkel, U. Hergenhahn, J. H. Sanchez, C. Hidalgo, K. P. Hollfeld, A. Hölting, D. Höschen, M. Houry, J. Howard, X. Huang, Z. Huang, M. Hubeny, M. Huber, H. Hunger, K. Ida, T. Ilkei, S. Illy, B. Israeli, S. Jablonski, M. Jakubowski, J. Jelonnek, H. Jenzsch, T. Jesche, M. Jia, P. Junghanns, J. Kacmarczyk, J.-P. Kallmeyer, U. Kamionka, H. Kasahara, W. Kasparek, N. Kenmochi, C. Killer, A. Kirschner, T. Klinger, J. Knauer, M. Knaup, A. Knieps, T. Kobarg, G. Kocsis, F. Köchl, Y. Kolesnichenko, A. Könies, R. König, P. Kornejew, J.-P. Koschinsky, F. Köster, M. Krämer, R. Krampitz, A. Krämer-Flecken, N. Krawczyk, T. Kremeyer, J. Krom, I. Ksiazek, M. Kubkowska, G. Kühner, T. Kurki-Suonio, P. A. Kurz, M. Landreman, P. Lang, R. Lang, S. Langish, H. Laqua, R. Laube, S. Lazerson, C. Lechte, M. Lennartz, W. Leonhardt, C. Li, C. Li, Y. Li, Y. Liang, C. Linsmeier, S. Liu, J.-F. Lobsien, D. Loesser, J. L. Cisquella, J. Lore, A. Lorenz, M. Losert, A. Lücke, A. Lumsdaine, V. Lutsenko, H. Maaßberg, O. Marchuk, J. H. Matthew, S. Marsen, M. Marushchenko, S. Masuzaki, D. Maurer, M. Mayer, K. McCarthy, P. McNeely, A. Meier, D. Mellein, B. Mendelevitch, P. Mertens, D. Mikkelsen, A. Mishchenko, B. Missal, J. Mittelstaedt, T. Mizuuchi, A. Mollen, V. Moncada, T. Mönnich, T. Morisaki, D. Moseev, S. Murakami, G. Náfrádi, M. Nagel, D. Naujoks, H. Neilson, R. Neu, O. Neubauer,

T. Ngo, D. Nicolai, S. K. Nielsen, H. Niemann, T. Nishizawa, R. Nocentini, C. Nührenberg, J. Nührenberg, S. Obermayer, G. Offermanns, K. Ogawa, J. Ölmanns, J. Ongena, J. W. Oosterbeek, G. Orozco, M. Otte, L. P. Rodriguez, N. Panadero, N. P. Alvarez, D. Papenfuß, S. Paqay, E. Pawelec, T. S. Pedersen, G. Pelka, V. Perseo, and the W7-X Team, "Demonstration of reduced neoclassical energy transport in wendelstein 7-x," Nature **596**, 221–226 (2021).

[49]D. Moseev, R. Ochoukov, V. Bobkov, R. O. Dendy, H. Faugel, D. Hartmann, J.-P. Kallmeyer, J. Lansky, H. P. Laqua, S. Marsen, K. G. McClements, S. K. Nielsen, A. Reintrog, M. Salewski, B. S. Schmidt, T. Schulz, and T. Stange, "Development of the ion cyclotron emission diagnostic for the w7-x stellarator," Review of Scientific Instruments **92**, 33546 (2021).

[50]O. Samant, R. O. Dendy, S. C. Chapman, D. Moseev, and R. Ochoukov, "Predicting ion cyclotron emission from neutral beam heated plasmas in wendelstein7-x stellarator," Nuclear Fusion **64**, 056022 (2024).

[51]Y. I. Kolesnichenko, V. V. Lutsenko, and A. V. Tykhyy, "Ion cyclotron emission in maxwellian plasmas," Physics of Plasmas **31**, 042107 (2024).

[52]G. H. DeGrandchamp, W. W. Heidbrink, X. D. Du, J. B. Lestz, E.-H. Kim, S. Shiraiwa, M. A. V. Zeeland, J. A. Boedo, K. E. Thome, N. A. Crocker, and R. I. Pinsker, "Propagation of ion cyclotron emission in the diii-d tokamak," Physics of Plasmas **32**, 032508 (2025).

[53]E. Westerhof, J. W. Oosterbeek, M. D. Baar, M. A. van den Berg, W. Bongers, A. Bürger, M. F. Graswinckel, R. Heidinger, B. Hennen, J. A. Hoekzema, S. B. Korsholm, O. G. Kruijt, B. Lamers, F. Leipold, S. K. Nielsen, D. Thoen, B. C. E. Vaessen, and P. M. Wortman, "The textor line-of sight ece system for feedback controlled ecrh power deposition," in *35th EPS Conference on Plasma Physics* (2008) p. P1.081.

[54]S. K. Nielsen, M. Salewski, W. Bongers, S. B. Korsholm, F. Leipold, F. Meo, P. Michelsen, D. Moseev, J. W. Oosterbeek, M. Stejner, and E. Westerhof, "Modification of the collective thomson scattering radiometer in the search for parametric decay on textor." The Review of scientific instruments **83**, 113508 (2012).

[55]E. Gusakov and A. Popov, "Low threshold parametric decay backscattering instability in tokamak electron cyclotron resonance heating experiments," Physical Review Letters **105**, 115003 (2010).

[56]E. Z. Gusakov and A. Y. Popov, "Theory of anomalous backscattering in second harmonic x-mode ecrh experiments," Physics of Plasmas **23**, 082503 (2016).

[57]A. Tancetti, S. K. Nielsen, J. Rasmussen, D. Moseev, T. Stange, S. Marsen, M. Vecséi, C. Killer, G. A. Wurden, T. Jensen, M. Stejner, G. Anda, D. Dunai, S. Zoletnik, K. Rahbarnia, C. Brandt, H. Thomsen, M. Hirsch, U. Hoefel, N. Chaudhary, V. Winters, P. Kornejew, J. Harris, H. P. Laqua, and T. W.-X. Team, "Inhibition of parametric decay in heating microwave beams during fluctuations of the density profile in the edge island of wendelstein 7-x," Plasma Physics and Controlled Fusion **65**, 015001 (2023).